A Cooperative Atmosphere–Surface Exchange Study (CASES) Dataset for Analyzing and Parameterizing the Effects of Land Surface Heterogeneity on Area-Averaged Surface Heat Fluxes

DAVID N. YATES,*,+ FEI CHEN,* MARGARET A. LEMONE,* RUSSELL QUALLS,+,# STEVEN P. ONCLEY,* ROBERT L. GROSSMAN,@ AND EDWARD A. BRANDES*

* *National Center for Atmospheric Research,*& *Boulder, Colorado*
+ *Department of Civil Engineering, University of Colorado, Boulder, Colorado*
# *Department of Biological and Agricultural Engineering, University of Idaho, Moscow, Idaho*
@ *Program in Atmospheric and Oceanic Science, University of Colorado, Boulder, Colorado*

(Manuscript received 25 January 2000, in final form 21 August 2000)

ABSTRACT

A multiscale dataset that includes atmospheric, surface, and subsurface observations obtained from an observation network covering a region that has a scale order comparable to mesoscale and general circulation models is described and analyzed. The dataset is half-hourly time series of forcing and flux response data developed from the one-month Cooperative Atmosphere–Surface Exchange Study (CASES-97) experiment, located in the Walnut Watershed near Wichita, Kansas. The horizontal complexity of this dataset was analyzed by looking at the sensible and latent heat flux response of station data from the three main land surface types of winter wheat, grass/pastureland, and bare soil/sparse vegetation. The variability in the heat flux response at and among the different sites points to the need for a spatially distributed, time-varying atmospheric-forcing dataset for use in land surface modeling experiments. Such a dataset at horizontal spacings of 1, 5, and 10 km was developed from the station data and other remotely sensed platforms, and its spatial heterogeneity was analyzed.

1. Introduction

Knowledge of the two-way interactions between atmospheric and land surface processes is crucial to our understanding of weather, climate, and river basin hydrology (e.g., Charney et al. 1977; Pan and Mahrt 1987; Liang et al. 1994; Schaake et al. 1996). Recent research (e.g., Betts et al. 1996; Segal et al. 1988; Wood et al. 1992; Chen et al. 1997, 1998; Zhong and Doran 1998) shows that a sound land surface model, providing more accurate estimates of surface heat fluxes, can improve the medium- and short-term numerical weather forecasts of precipitation and near-surface weather variables. These improvements are complicated by the fact that the natural land surface is heterogeneous because of variations in soils, vegetation, and topography. The horizontal grid spacings of 30–100 km in current and near-future atmospheric general circulation models (GCMs) and mesoscale models cannot adequately resolve these land surface variabilities. Improving the representation of subgrid-scale variability in land surface models (LSM) remains a challenge for large-scale atmospheric–hydrological modeling.

The extent to which subgrid-scale surface heterogeneity affects the surface heat flux calculation has been strongly debated. For example, Avissar and Pielke (1989), Bonan et al. (1993), Chen and Avissar (1994a,b), and Grotzer et al. (1996) have shown that subgrid-scale surface heterogeneity and its associated subgrid-scale processes have significant influences on processes at meso and GCM scales. These land surface effects cannot be resolved using grid-averaged values, yet they need to be represented in these large-scale models (Gao 1995). On the other hand, Garratt et al. (1990) and Wood and Lakshmi (1993) have suggested that these processes can be represented at the larger scale using grid-averaged effective parameters. For example, the major result of Wood and Lakshmi (1993) was that fluxes and surface characteristics essentially scale linearly. In another study, Sellers et al. (1995) concluded that using mean values of topography, vegetation conditions, and soil moisture to calculate the surface heat fluxes is sufficient for mesoscale atmospheric models.

A modeling study by Avissar and Schmidt (1998) suggested that landscape ''patchiness,'' with character-

& The National Center for Atmospheric Research is sponsored by the National Science Foundation.

Corresponding author address: David N. Yates, NCAR/RAP, P.O. Box 3000, Boulder, CO 80307-3000.
E-mail: yates@ucar.edu

istics lengths of less than 5–10 km, does not significantly affect the convective boundary layer. However, a conceptually similar modeling experiment by Shen and Leclerc (1995), who used 250-, 500-, and 1000-m sinusoidal surface heat flux variance, found that even small horizontal surface inhomogeneities influence the horizontally averaged variances, covariances, and third moments. Experimental design and validation of modeling experiments, such as those by Avissar and Schmidt (1998) and Shen and Leclerc (1995), would be improved from the dataset described in this paper.

Regardless of these different debates, developing approaches to represent subgrid-scale variability effects in atmospheric–hydrological models has been a focus of recent studies (e.g., Avissar and Pielke 1989; Entekhabi and Eagleson 1989; Claussen 1991; Pielke et al. 1991; Koster and Suarez 1992; Famiglietti and Wood; 1991; Bonan et al. 1993; Avissar and Chen 1993; Li and Avissar 1994; Lakhtakia and Warner 1994; Chen and Avissar 1994a; Gao 1995). A fundamental issue of these debates and modeling approaches is how to verify the different methods and their associated outcomes. Verification requires a multiscale dataset that includes atmospheric, surface, and subsurface observations from an observation network covering a region that has a scale order comparable to meso- and GCM scales.

Only a few studies have used observations to validate theories and models. Smith et al. (1992) and Sellers et al. (1995) utilized the First International Land Surface Satellite Climatology Project Field Experiment (FIFE) observations to investigate the effects of spatial variability in topography, vegetation cover, and soil moisture on area-integrated surface fluxes. However, the FIFE experimental area only covered a small domain (15 km $\times$ 15 km) dominated by grass. As such, their conclusions may not be applicable to generalized (or more complex) inhomogeneous situations. Ghan et al. (1997) and Doran et al. (1998) describe a dataset over the U.S. Department of Energy's Atmospheric Radiation Measurement Program (ARM) Clouds and Radiation Test Bed (CART) in Kansas and Oklahoma. Their domain was large (300 km on a side) and consisted of half-hourly, gridded (6.25 km) data derived from measurements of over 100 stations, and precipitation was derived from Next-Generation Radar (NEXRAD) stage-III data at 4.7-km resolution. The dataset developed by Ghan et al. (1997) and Doran et al. (1998) is conceptually similar to the one described here, but this paper additionally describes and analyzes the variability of the surface observations. This information should prove useful to the atmospheric and hydrologic science communities who use this dataset. Also, this dataset includes more detailed estimates of the spatial and temporal varying precipitation fields, which is important given the fact that variations in surface hydrologic processes give rise to contrasts in sensible and latent heat flux. The dataset includes high-resolution, gauge-corrected quantitative precipitation estimates (QPEs) from the National Center for Atmospheric Research's (NCAR) dual-polarization weather radar of the major storm events, and NEXRAD stage-III QPEs were used to complete the dataset.

CASES-97 was a one-month field campaign of the multiyear Cooperative Atmosphere–Surface Exchange Study (CASES). The CASES study region is located in the Walnut River watershed region of central Kansas, covering roughly 3600 km^2, with approximately 200 m of elevation relief from the northeastern headwaters of the Walnut to its confluence with the Arkansas River to the south (Fig. 1). The study region was selected because of unique geographic characteristics (varying topography and multiple land use types) and hopes to serve as a long-term site for understanding the complex interactions among meteorological, climatological, hydrological, ecological, and environmental chemical factors. It also provides an excellent test bed for validating different approaches for estimating area-integrated heat fluxes at meso- and GCM scales [details could be found at the time of writing at http://www.joss.ucar.edu/cases/ and in Lemone et al. (1998, 2000)].

In section 2, we briefly describe the CASES-97 field experiment and measured atmospheric and surface data. In section 3, we analyze the surface response data, with a particular focus on the variability of sensible and latent heat flux between and among the various stations. Analysis of site data is important because these data can be used to develop and compare different land surface parameterization schemes within land surface models. Although these models are executed over a continuous domain, point estimates of surface heat fluxes can be used for model verification. Therefore, the variability of the station data is both qualitatively and quantitatively described and analyzed. A spatial and temporal varying atmospheric forcing dataset, based on the station data are described in section 4. Section 5 includes general comments and conclusions regarding the variability of the heat flux data and the spatially distributed surface and time-varying atmospheric forcing datasets from the CASES-97 experiment.

2. The CASES-97 field experiment

Apart from the surface heat flux and atmospheric data that are the focus of this paper, the CASES-97 experiment (covering the period from 0000 UTC 21 April to 2345 UTC 22 May 1997) included other data-gathering platforms [see Lemone et al. (2000) for details]. Briefly, these included Doppler radar profilers that measured wind speeds, radioacoustic sounding system virtual temperatures, and estimates of planetary boundary layer (PBL) depth. Two aircraft platforms, the National Science Foundation/University of Wyoming King Air and the National Oceanic and Atmospheric Administration/Aircraft Operations Center (NOAA/AOC) Twin Otter, measured atmospheric temperature, humidity, pressure, wind speeds, up- and downwelling short- and longwave

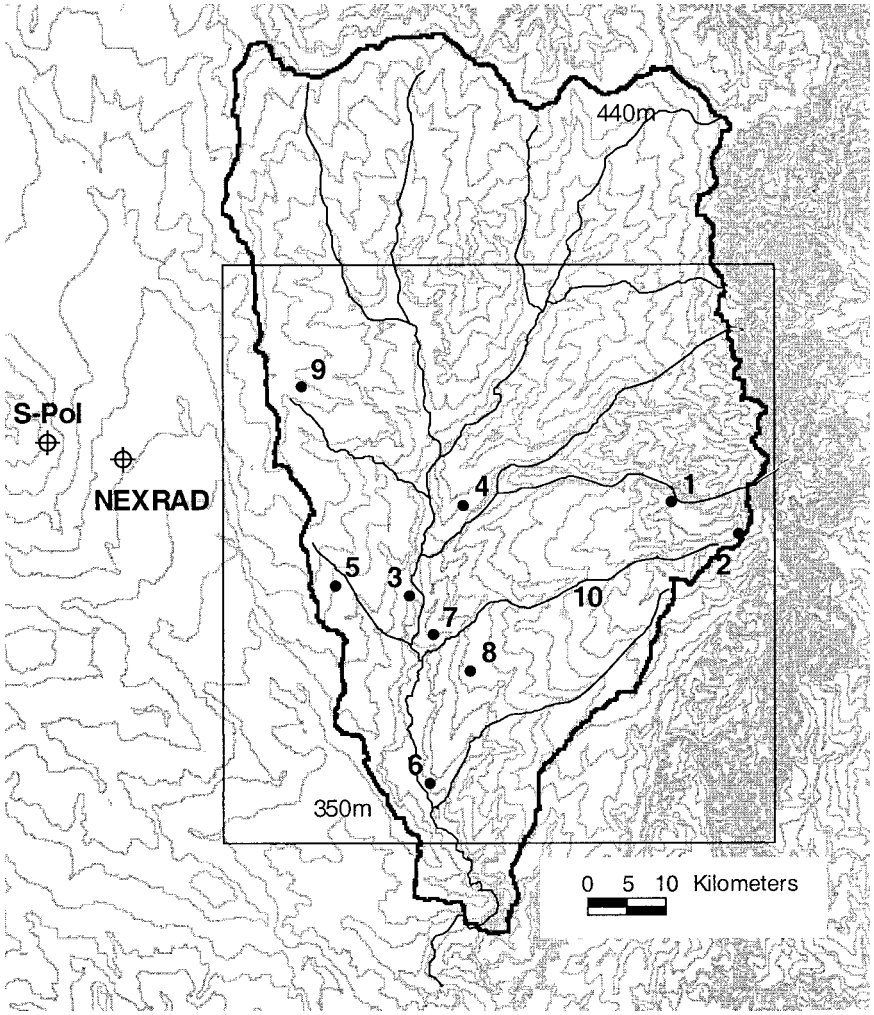

FIG. 1. The Walnut River watershed (thick dark line), elevation contours (light thin lines), the 74 km × 71 km domain (thin dark line), the location of the surface flux stations (sites 10 was not part of the official CASES experiment), and the weather radars. Contour intervals are 10 m.

radiation, and other constituents. NCAR's S-band polarized radar system (S Pol) determined precipitation type as well as rate and Doppler air motion for several storms. Long-term observational instruments were also established to support the ARM CART facilities at three sites (Lemone et al. 2000).

Continuous data were collected from nine surface flux stations for the duration of CASES-97 and from a 10th station from 5 to 20 May. The numbers in Fig. 1 denote the surface flux stations, located so that they represented the main topographic and land use/land cover features of the area (Table 1). Stations 1–6 were portable automated mesonet (PAM) sites, stations 7 and 8 were Atmosphere–Surface Turbulent Exchange Research Sites (ASTER) sites, station 9 (operated by NCAR) was set up by R. Qualls from the University of Colorado, and station 10 was supplied by NOAA's Atmospheric Turbulence and Diffusion Division.

These stations sampled the complete surface energy budget using eddy correlation techniques, momentum fluxes, temperature, wind, pressure, rainfall, radiation, and radiometric surface temperatures (LeMone et al. 2000). The instruments were mounted to ensure good exposure to the prevailing wind speeds, SE–S–SW and NW–N, with the tower ''shadow'' toward the southeast. Fetches for these winds generally were at least 200 m. Soil moisture and temperature were sampled continuously at ~5 cm below the surface. The data used here are at 0.5-h intervals but are available at 5-min resolution. Roughly once a week, soil moisture profiles were sampled at 5-cm intervals down to 70 cm at station 7 and to 110 cm at station 8. Surface characteristics (a description of ground cover and photographs in the four cardinal directions) were documented at stations 1–9 on 20 April, 1 May, 12 May, and 20 May (Table 2).

TABLE 1. Land surface characteristics at each station. The ''General'' column describes the three broad land classes that were combined for the aggregate analysis. *Site 9 was set up by R. Qualls of the University of Colorado, but the site was maintained by NCAR during the field experiment.

Site	Elevation	Instrument	General	Specific land characterization
1	464	PAM	Grass/pasture	Pasture/rangeland
2	478	PAM	Grass/pasture	High grass
3	360	PAM	Bare soil/sparse vegetation	Tilled field: new corn/beans
4	381	PAM	Bare soil/sparse vegetation	Low crop of milo stubble/rangeland
5	390	PAM	Winter wheat	Tilled field: broadcast spread wheat
6	351	PAM	Winter wheat	Winter wheat in floodplain
7	363	ASTER	Winter wheat	Winter wheat, wide rows
8	384	ASTER	Grass/pasture	Grassland, big bluestem
9*	424	PAM	Grass/pasture	Grassland

3. Analysis of surface flux data

Apart from the large-scale diurnal variation and instrument measuring biases, two major components contribute to withinday and day-to-day heat flux variability: 1) variability in the *atmospheric forcing* (primarily due to horizontal gradients of precipitation, wind speed, humidity, surface radiation related to changes in cloud cover, etc.) and 2) variability of the *land surface* characteristics (vegetation distribution; soil moisture; soil texture, color, and hydraulic properties; and topography, including slope, aspect, and relative elevation). The major factors that led to variability in the observed heat flux among the different CASES-97 surface measuring stations were examined, including the influence of cloudiness, precipitation/soil moisture, and land cover.

To understand surface factors that led to the observed flux variance, a distinction was made between cloudy and noncloudy days and the primary land cover type (winter wheat, bare soil/sparse vegetation, and grass/pastureland). Clouds exert a major control on the surface radiation components. In fact, Smith et al. (1992) found for FIFE that the standard deviation of heat flux for a composite diurnal cycle that included cloudy days was more than twice that of an average diurnal cycle composed only of clear days. In addition, the surface heat fluxes during the drydown process immediately following a rainstorm were examined to compare the heat flux responses as a function of the land cover type and the evolving surface characteristics.

a. Uncertainty in surface flux data

Knowing the uncertainty in surface heat flux measurements is critical to the data analysis process and to subsequent land surface modeling validation experiments. Both observational and numerical modeling studies have shown that significant heat flux gradients can influence the evolution of the PBL (Yan and Anthes 1988; Wang and Paegle 1996; Pielke et al. 1991). Measurement uncertainty of surface energy components at CASES-97 was, in some cases, on the order of 100 W m^{-2}, suggesting that results from future LSM experiments should not necessarily be directly compared with CASES-97 observations (this outcome highlights the need for improved measurement techniques that preserve the surface energy balance).

The primary interest, however, was the examination of the relative variability of the surface heat flux at and

TABLE 2. Surface data in CASES-97 used for gridded dataset; station 10 was only used in validation [see Lemone et al. (2000) for details].

Variable	Stations 1–6	Station 8	Station 7	Station 9	Station 10
Pressure	Vaisala 200 barometer	Same	Same	Not measured	Vaisala
Surface air temperature	Vaisala 50Y	NCAR/SSS F-Vaisala	NCAR/SSS F-Vaisala	REBS THP with aspirated shield	Vaisala 50Y
Specific humidity	Vaisala 50Y	NCAR/SSS F-Vaisala	NCAR/SSS F-Vaisala	REBS THP	Vaisala HMP35D
Zonal wind (u) and meridional wind (v)	R.M. Young 5103 propeller vane	Same	Same	R.M. Young cup anemometer	R.M. Young bivane
Surface temperature	Everest radiometer at 45°	Same	Same	EI-Infrad transduce (4000.4GL)	Not measured
Soil moisture	Campbell Scientific (~5 cm)	Dielectric, TRIME (+profiles, see text)	Dielectric, TRIME	REBS SMP 1 (4 cm)	Vitel hydra
Soil temperature	REBS (2–8 cm)	Micromet Systems	Micromet Systems	REBS STP-1 (4 cm)	ATDD
*Precipitation	Tipping bucket, MRI	Tipping bucket, MRI	Tipping bucket, MRI	Not measured	Met One rain gauge

* Primary data are radar-based rainfall estimates.

TABLE 3. Surface flux data in CASES-97.

Variable	Stations 1–6	Station 8	Station 7	Station 9	Station 10
Downward shortwave radiation	LI-COR	Same	Same + Eppley PSP	From neighbor stations	LI-COR LI-200 SB
Downward Longwave	Estimated (see text)	Same	Eppley precision IR pyrgeometer	Estimated	Estimated
Net radiation	REBS	REBS	Micromet Systems	REBS Q*7	REBS Q*7
Sensible heat flux	Sonic anemometer	Same	Applied Tech. sonic	Campbell Scientific 1-D sonic/thermocouple (CA27)	Gill ''Solent'' 3D sonic anemometer
Latent heat flux	Sonic + uv hygrometer + H (see text)	Same	Ophir IR + sonic	LE = $R_n - H - G$	ATDD infrared gas analyzer IRGA) + sonic
Soil heat flux	Flux plate (REBS)	Flux plate (Micromet Systems)	Same	Flux plate (REBS HFT3)	Flux plate (REBS)
Momentum flux	Sonic	Sonic	Sonic	None	Sonic

among the different sites. Because the surface stations used the same techniques to estimate heat flux terms, self-consistency should be expected among the measurements, and, if there was a bias, it should be systematic. Tables 2 and 3 detail, by station, the basic surface meteorological and flux data used to produce the surface dataset. The utilization of this dataset should improve our understanding of the role of surface variability, even if it is in a relative sense.

There were two possible measurement error sources for the surface heat fluxes. One was related to the individual field measurements of temperature, humidity, wind speed, vertical moisture, and momentum fluxes, and so on, and the other was related to the techniques used to derive surface heat fluxes. Such uncertainties are a function of instrument accuracy, fetch, and representativeness of the measurements.

1) RADIATION

Absolute accuracy for the downwelling shortwave radiation for stations 1–8 is 5%; comparison of ratios of the LI-COR, Inc., instruments at these stations to the precision spectral pyrheliometer (PSP) at station 7 to collocated measurements obtained two years after the field program suggest that (a) for ''golden'' days, the PSP could be used to represent downwelling solar radiation over the day, and (b) for partly cloudy days, the golden-day ratios could be used to correct the downwelling solar radiation at these stations.

2) NET RADIATION

The quoted error for net radiation is 5%. A comparison of net radiation from the NCAR sites to those at site 10 (the NOAA site) and the fact that the surface energy budget did not balance at most of the NCAR sites suggest that NCAR estimates of net radiation had a high bias of between 5% and 10%. Goutorbe (1992) notes that net radiometers can show significant discrepancy in their estimate of net radiation.

3) SURFACE HEAT FLUXES

Sensible heat flux was found by eddy correlation using fast-response instrumentation (Table 2) and corrected for sonic tilt errors. The latent heat flux for station 10 was found through simple eddy correlation. At stations 1–8, the flux estimate relied on an assumption of spectral similarity [the ratio of the integrated flux over a frequency band for which both the temperature and moisture instruments work well (Horst and Oncley (1995)], along with high-frequency temperature fluctuations, to estimate the high-frequency humidity flux. At station 9, the latent heat flux was found from net radiation, soil heat flux, and sensible heat flux, as a residual to the surface energy budget. Soil heat fluxes were measured with similar instruments. As in the case of net radiation, this measurement represents an area much smaller than the eddy-correlation-based fluxes.

4) SURFACE ENERGY BALANCE

To assess the accuracy of the surface energy balance, the surface heat flux residual was estimated. Heat flux residuals R_f were estimated as the difference between observed net radiation and the sum of sensible H, latent LE, and surface G heat fluxes: $R_f = R_n e - (H + \mathrm{LE} + G)$. Ideally R_f should equal zero, where independent measurements of net radiation would cancel the summed ground, sensible, and latent heat fluxes.

Site 9 only measured net radiation and used the surface energy budget to compute latent heat flux; site 10 was an independent site set up by NOAA. Of the stations independently measuring all terms in the surface heat budget, station 10 came closest to balancing. Sites 2 and 7 showed the greatest amount of error in their surface energy balance. Site 2 (a grass site) had a residual error of approximately 100 W m^{-2}, and a comparison with the other grass sites suggests an underestimation of the surface heat flux. Site 7 (a winter wheat site) experienced intermittent instrument failure during portions of the experiment, so its energy balance was computed over fewer days. With the exception of sites 2 and 7,

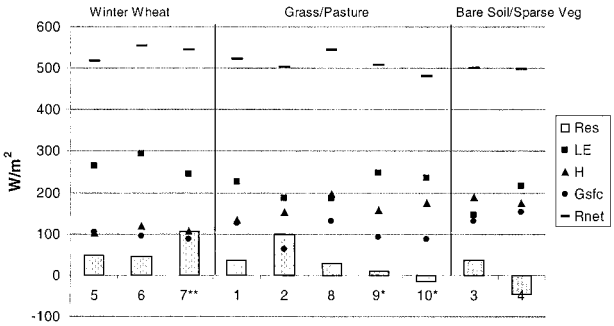

FIG. 2. The 6-h daytime average of the surface heat flux components for the period of 3–15 May, which corresponded to the observing period of station 10*, which was an independent NOAA site.* The latent heat flux at station 9 was computed from the energy balance equation, LE = $R_n - H - G$, so although the surface energy should exactly balance, the small residual error was due to missing data at station 9 that was filled with surrounding station data. ** The average energy balance at station 7 was computed only over 9 days because of missing data as a result of instrument failure.

the average R_f around solar noon was approximately 50 W m^{-2} (Fig. 2). The latent and surface heat fluxes likely represent the largest sources of error in the energy heat budget calculations. The surface heat flux was computed from estimates of soil heat flux plus heat storage determined from soil temperature and moisture measurements. Particularly, soil moisture estimates required empirical calibrations, and latent heat estimates included instrument corrections such as sonic anemometer tilt, ''oxygen correction'' from krypton hygrometer values, and Webb corrections.

b. Flux variance of the three land use types

Figures 3 and 4 are plots of the 6-h daytime average and the standard deviation (departure from the mean) of LE based on clear-sky and near-clear-sky days (henceforth, ''clear-sky and near-clear-sky'' are referred to as ''clear-sky'' only) and the complete 32-day period[1] (referred to as the composite) for all sites, respectively. Clear-sky days were determined through an objective, day-to-day examination of the incoming solar radiation. If the ratio of the sum of the observed incoming solar radiation and the sum of the theoretical clear-sky incoming solar radiation was greater than 90%, then the day was classified as clear-sky. Figures 5 and 6 are similar to Figs. 3 and 4, except they are for *H*. These data were derived for each site by averaging over a 6-h period around solar noon (1230 CST). The four figures suggest day-to-day variability at individual sites on the basis of their standard deviations and suggest spatial differences among the sites on the basis of their means.

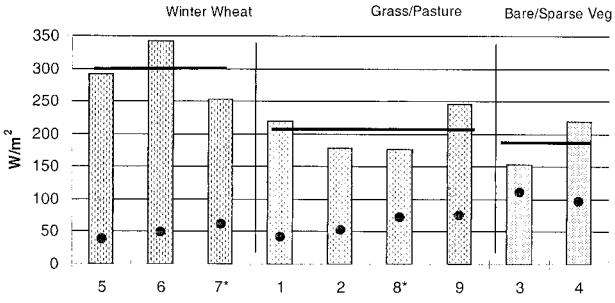

FIG. 3. Station latent heat flux based on a 6-h average around solar noon (bar) and the standard deviation (dark dot within bar) during 13 clear- and near-clear-sky days (except for sites 7 and 8, where only 9 and 12 days were used, respectively, because of instrument failure). The three horizontal black lines are the average values computed for each site type. Site 9 is shaded because it was set up by the University of Colorado but managed by NCAR, it had a different array of measuring equipment, and different techniques were used to estimate the surface energy balance at this site.

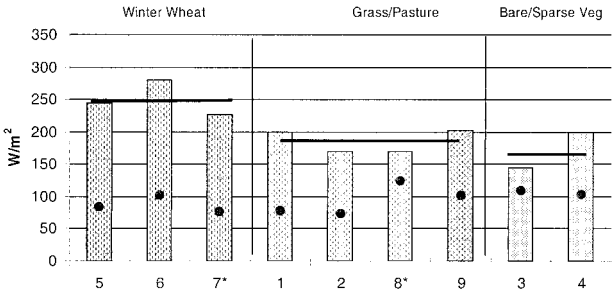

FIG. 4. Same as Fig. 3, but a 25-day composite of both clear-sky and cloudy days.

1) SITES 5, 6, AND 7 (WINTER WHEAT)

Sites 5, 6, and 7 (Fig. 1) were planted in winter wheat, each with unique characteristics. Site 5 was ''randomly'' planted using a broadcast seed application technique with an average crop height of about 30 mm at the start of the experiment. Site 6 was situated in the floodplain of the Walnut River and was planted in tightly spaced rows with the greatest crop height during the experiment. Winter wheat at site 7 was in rows but with a

[1] Although the surface stations recorded continuously for a 32-day period, heat flux estimates were made for only 25 of the 32 days, because days with rain or forecasts of rain required the placement of bags on the heat flux measuring equipment, rendering the heat flux data on ''bagged'' days useless.

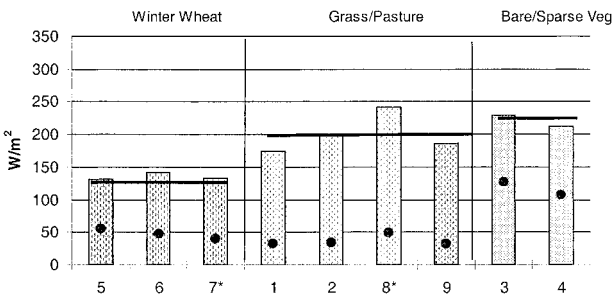

FIG. 5. Same as Fig. 3, but for sensible heat flux.

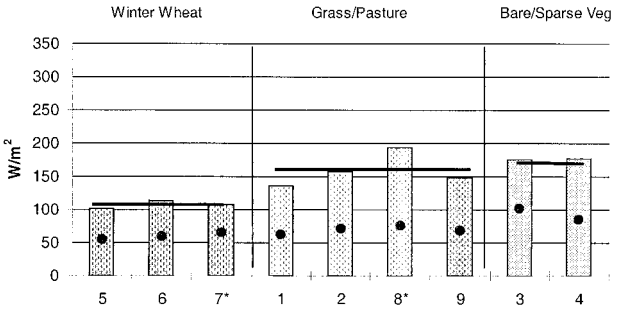

FIG. 6. Same as Figure 4, but for sensible heat flux.

significantly greater spacing (50–60 cm) when compared with site 6. Sites 5, 6, and 7 received precipitation totals of 143, 70, and 127 mm, respectively. The 30-yr average precipitation over the period of 21 April–22 May for Wichita, Kansas, (located just to the west of the CASES domain) is roughly 70 mm.

The smaller LE for clear-sky days at site 7 as compared with sites 5 and 6 was consistent with site observations, because site 7 had more exposed soil due to wider crop spacing (Fig. 3). The exposed soil influenced the partitioning of the latent and sensible heat, leading to a higher Bowen ratio ($b = H/\mathrm{LE}$) as compared with sites 5 and 6. Site 6, situated in the floodplain and with tall, dense plant cover, had the highest average LE. Generally, site 6 was more photosynthetically active, had a rougher surface, and had more active surface energy exchanges.

When cloudy days were included in the analysis, the mean value of the peak latent heat flux dropped about 75 W m^{-2} and the standard deviation nearly doubled (Fig. 4). The actual reduction and variability of latent heat flux during cloudy days is likely greater because data for several cloudy days was rejected because the instruments were forced offline (see footnote 1). For the composite day (Fig. 4), the relative difference between the 6-h daytime average LE for the wheat sites was small (between 25 and 50 W m^{-2}), because clouds reduced the evaporative demand of the atmosphere.

Plots of the sensible heat flux (Figs. 5 and 6) for the winter wheat told a story broadly similar to that of latent heat flux, except that the magnitude and variance of H among the three winter wheat sites was lower for the 6-h daytime averages. Variability of the sensible heat flux from the plant canopy is reduced because the surrounding plant matter acts as an insulating agent.

2) SITES 1, 2, 8, AND 9 (PASTURE/GRASSLAND)

Sites 1, 2, 8, and 9 were located in grass and pastureland (Fig. 1). Sites 1 and 2 were in an area with more topographic relief relative to the other sites, with site 2 near a ridgetop and better drained than site 1. The composition of grasses at site 8 was more diverse when compared with the other grass sites. Site 9 was poorly drained and had relatively uniform grasses. All four grass sites underwent increases in photosynthetic activity over the course of the 32-day field campaign. Because site 9 used a different method to compute its heat flux components, the comparison and relevant discussion are limited to sites 1, 2, and 8 only.

Figures 3 and 4 show that the 6-h daytime-average LE of grass was, on average, smaller and, in some cases, had a higher variance in comparison with winter wheat. Under clear skies, the midday deviation of LE among sites 1, 2, and 8 was as much as 45 W m^{-2} (between sites 1 and 8). Site 2 (better drained) and site 8 had a smaller green fraction (less photosynthesizing vegetation), leading to smaller latent heat fluxes. Among the sites, cloud cover systematically reduced the magnitude but increased the variability of the surface heat (Figs. 4 and 6).

The sensible heat flux at site 8 was consistently greater than the other grass sites (Figs. 5 and 6). The H at site 8 was about 50 W m^{-2} greater during peak daytime hours than the average for all grass sites under clear-sky conditions (Fig. 5) and 25 W m^{-2} greater for the composite 6-h daytime average (Fig. 6). One possible explanation is that site 8 had a larger fraction of brown, straw grass throughout the area, and thus less photosynthate and a consistently warmer surface. The standard deviations of the latent and sensible heat fluxes for all grass sites were broadly similar (comparing Figs. 3–6 for the grasses).

3) SITES 3 AND 4 (SPARSE VEGETATION/BARE SOIL)

Site 3 contained a large, bare area of newly planted corn and soy with an extending triangular area of winter wheat just to the east, and site 4 had a large tilled field of bare soil and crop residue to its south and sparse grass 8–10-cm high to its north. Although there was more vegetation surrounding the sites by the end of the experiment, the vegetation was still sparse in comparison with the other sites.

A comparison of sites 3 and 4 with the wheat and grass sites showed that the clear-sky 6-h daytime average LE was smaller, but the 6-h daytime standard deviation of LE was generally larger (Fig. 3). Site 4's latent heat flux was higher when compared with site 3, because more vegetation surrounded this site. In fact, the magnitude of site 4's LE during clear days was near that of some of the grass sites, although the variability of site 4's LE was higher. A significant portion of LE at sites 3 and 4 comes from the direct evaporation from bare soils, where water residing in the upper surface soil layer (i.e., less than 10 cm) immediately following a rain event is available for evaporation (Carlson et al. 1995). The greater variability of LE at sites 3 and 4 was attributed to the swift drying process immediately following a precipitation event. The rate of decline in LE following rain for the wheat and grass sites was smaller, because the plant canopy blocked incoming radiation to the ground surface, reducing evaporation.

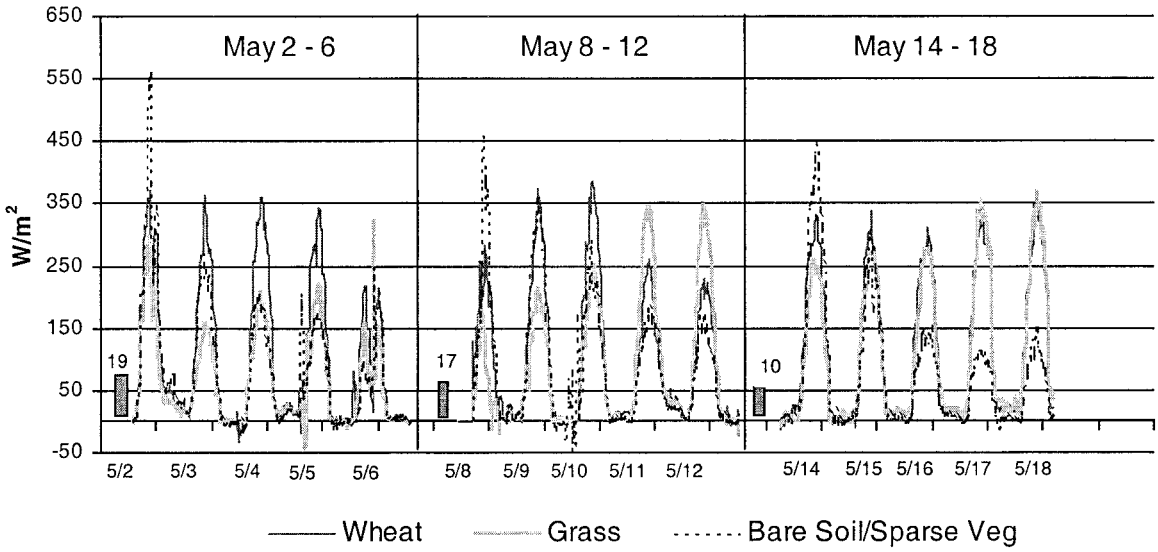

FIG. 7. Plot of latent heat flux for the three major land use classes (computed as an average for the land use type) during drydown periods following three major precipitation events in May. The bar inside the graph is the average gauge precipitation (mm).

For sites 3 and 4, cloud cover reduced the magnitude of the heat fluxes and increased its standard deviation, but by a smaller percentage when compared with the wheat and grass sites (Figs. 4 and 6). For these two sites, the standard deviation of the clear-sky and composite 6-h daytime LE differed by only 20 W m^{-2} (Figs. 3 and 4). The wetting–drying process of the bare soil/sparse vegetation sites led to as much variance in heat flux as did variance attributed to the changing cloud cover.

4) DAY-TO-DAY AND WITHINDAY HEAT FLUX VARIABILITY

Figure 7 illustrates the drying rate of the different land cover types and the influence of the land cover on the surface heat flux. The three series are land cover specific and were derived by averaging the sites—winter wheat (an average of sites 5, 6, and 7), grass/pastureland (an average of sites 1, 2, 8, and 9), and bare soil/sparse vegetation (an average of sites 3 and 4). The plot shows that the latent heat flux for the bare soil was greater immediately following a storm and then rapidly declined as the surface dried. This result is in contrast to the wheat and grass sites, where the soil moisture in the root zone significantly controlled LE. In fact, for the second two events (8 May and 14 May), the LE during the drydown period for the vegetated sites increased (particularly for grass), suggesting increased photosynthetic and plant transpiration activity.

The change in the latent heat flux of grass reflects the important control of the photosynthetic process during the growing season. Even after the large 2 May precipitation event, LE from the grasses was small when compared with the latent flux from bare soil and wheat, because the grass surface was just beginning to green and was only moderately photosynthetically active. In spite of the abundance of available water and energy, evapotranspiration (and hence latent heat flux) remained low. The grass layer acted as a shield and prevented shortwave radiation from reaching the wet ground surface, and the inactive vegetation retarded the turbulent exchange of water vapor from the ground surface to the atmosphere (Bougeault 1991).

c. Scaling of surface heat fluxes

A key issue related to the parameterization of land surface heterogeneity in large-scale atmospheric models is the scaling property of surface energy variables. As the domain expands in size, variations in topography and atmospheric forcing might have a greater effect on the area-averaged heat flux. For example, Wood and Lakshmi (1993) used model results to suggest that surface heat fluxes are scale invariant. Yet this issue has not been fully addressed through the use of field observations because there have been few observational networks over a relatively large area (Ghan et al. 1997; Doran et al. 1998) and few distributed datasets. The CASES-97 field experiment covered an area of about 70 km $\times$ 70 km, and although the density of these surface stations is not ideal for studying all aspects related to the parameterization of surface heat fluxes, it still can provide insight into surface heat flux scaling.

Four sites (3, 5, 7, and 8) were selected within a 20 km $\times$ 20 km area (roughly the size of the FIFE study domain) to derive a spatially weighted, area-averaged flux time series of H and LE (small domain). Similarly, all nine sites were used to derive a spatially weighted, area-averaged heat flux time series for the entire study

TABLE 4. Percentage of land covered by the different surface types, given for the small domain (includes sites 3, 5, 7, and 8) and the large domain (includes all 9 sites). The fraction of bare soil/spare vegetation was estimated from field observations.

	Small domain	Large domain
Winter wheat	30%	25%
Grass/pastureland	50%	60%
Bare soil/sparse vegetation	20%	15%

area (large domain). In addition, an arithmetically averaged series of H and LE (an equal weighting of all nine sites) was computed. The percent area of each land cover for both the small and large domains is given in Table 4. Although these percentages do not differ greatly, the large domain included the two grass sites in the complex terrain and the winter wheat site in the floodplain.

Figures 8a,b compare the area-averaged latent heat flux of the small and large domains and show an approximate 40 and 10 W m^{-2} difference during daytime hours, for the clear and composite diurnal cycle, respectively. The magnitude of the variance between the small and large domains was nearly equal. Figures 9a,b compare the fractionally weighted, large domain with the arithmetically averaged series and show that an equal weighting of all sites produced a near-equal diurnal cycle, in both magnitude and variance, as compared with the diurnal cycle produced by weighting the stations according to their representative land class. This was true for both a clear and composite day.

4. Soil moisture

Sites 7 and 8 included continuous measurements of soil moisture at a depth of 10 cm and sampled soil moisture measurements between 10 and 100 cm during intensive observing periods. Figures 10a,b show the variation of soil moisture at 5-, 20-, and 65-cm depths. The near-surface soil moisture of both winter wheat and grass varies considerably, but the volumetric water content in the upper layers (both 5 and 20 cm) of the grass site was considerably higher than that of winter wheat. In addition to greater photosynthetic activity (and hence root water extraction), the winter wheat sites exhibited greater near-surface drainage from land tilling, which allowed for more rapid infiltration. Root depths at these two sites were not great. The deeper soil moisture (65

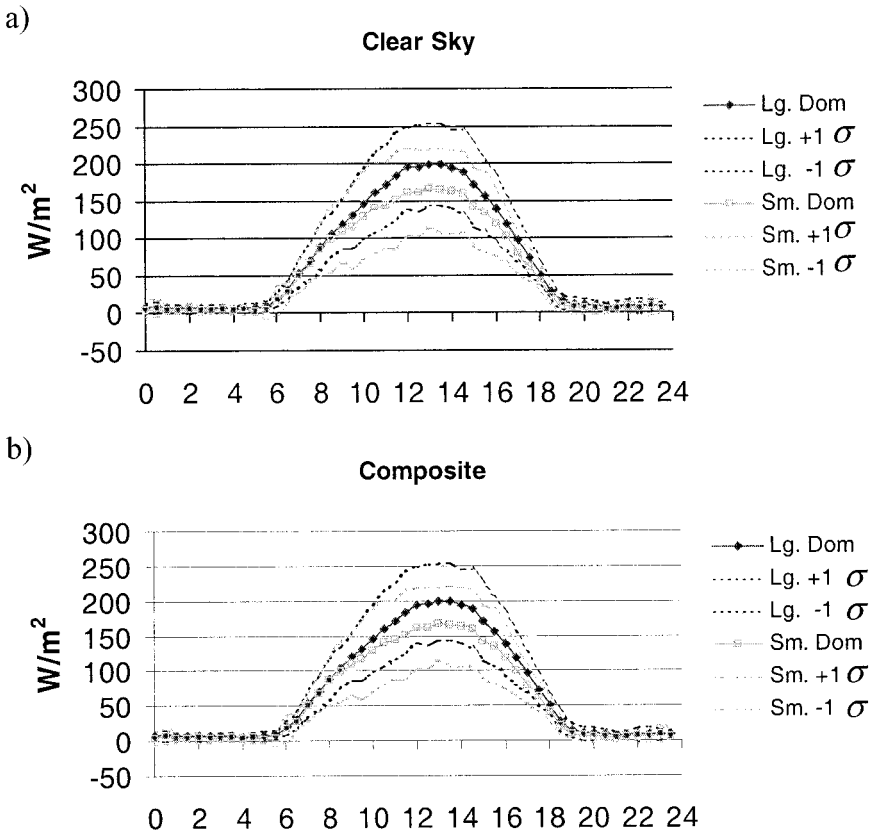

FIG. 8. (a) Average and standard deviation of the diurnal cycle of latent heat flux for clear- and near-clear-sky days based on a proportional weighting of the four sites that represented the small domain (Sm. Dom) and the nine sites that represented the large domain (Lg. Dom). (b) Same as (a), but for the composite 25 days.

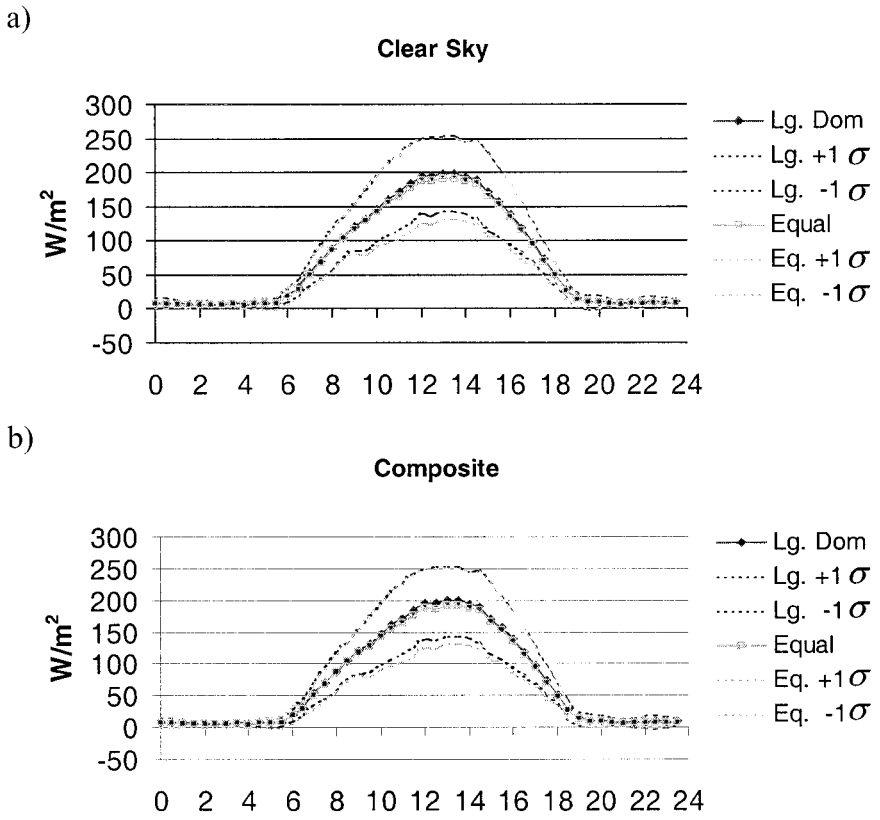

FIG. 9. (a) Average and standard deviation of the diurnal cycle of latent heat flux for clear- and near-clear-sky days based on equally weighting all sites (Equal) and weighting the nine sites according to their land cover (Lg. Dom). (b) Same as (a), but for the composite 25 days.

cm) of both wheat and grass were high (near saturation) and displayed similar variability.

5. A dataset for land surface modeling

The variability of surface heat fluxes is affected by a number of factors, because the area-averaging process depends on the land use type; the specific physical characteristics of the land surface such as soil moisture; and changes in the atmospheric forcing due to cloud cover, precipitation, temperature, wind, and so on. Small-scale features influence the area-averaged heat flux, but reproducing detailed patterns of spatial variability from station data is not possible because of the scale defined by the separation of sites.

As such, the density of the surface stations in CASES-97 is not suitable for conducting more detailed studies on the scaling of surface heat fluxes. The above analysis

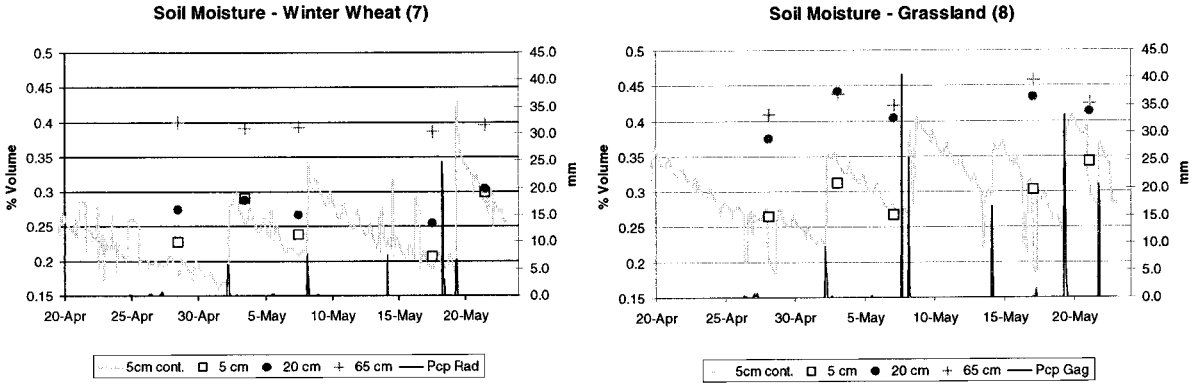

FIG. 10. Estimates of volumetric water content at sites 7 and 8 for depths of 5, 10, and 65 cm. Continuous measurements were made at 5 cm, and sample estimates were made during intensive observing periods.

of heat flux variability among observation sites is useful for model development and validation, but alternative approaches for generating flux maps with detailed horizontal variability should be investigated. This includes the use of high-resolution flux maps derived from satellites or generated from models.

To generate detailed surface heat flux maps from land surface models, a gridded, multiscale (with 1-, 5-, and 10-km resolution) dataset that includes atmospheric and surface data was developed from CASES-97 experimental data. The multiscale nature of the dataset will allow for comparative analysis of subgrid-scale analysis schemes, such as the ''mosaic approach'' (Avissar and Pielek 1989; Bonan et al. 1993), grid averaging, and others.

This dataset, in concert with station measurements, will serve future land surface modeling development and validation studies. Both gridded and station data were available at http://wwww.rap.ucar.edu/ as of the time of writing. Here, we will summarize the techniques used to develop the multiscale dataset based on the surface station measurements, radar rainfall estimates, and surface characteristic fields.

To create the gridded dataset, a serially complete time series of the atmospheric forcing variables was first created by filling missing station data. For stations with missing data of less than 3 h and if the missing data did not span an inflection point in the diurnal cycle, the station data were simply filled through a linear interpolation between the data at the beginning and end of the missing period. For stations missing data over longer periods or missing data that spanned an inflection point in the diurnal cycle, data were filled based on a relative distance weighting of the surrounding stations of the same land cover type. Of the nine atmospheric forcing variables listed in section 2, two of those variables, longwave downward radiation and precipitation, require additional discussion. The other seven surface station data variables were quality checked and made continuous with a time interval of 30 min.

a. Downward longwave radiation

Only site 7 directly measured longwave downward radiation L_d during the CASES-97 field program. For the other eight stations, half-hourly values of L_d were computed by

$$L_d = R_n + L_u - S_d(1 - \alpha), \tag{1}$$

where measured variables included net radiation R_n and shortwave downward radiation S_d (except for site 9). Longwave upward radiation L_u was computed by $L_u = \varepsilon_s \sigma T_s^4$, where ε_s is the surface emissivity (0.96), σ is the Stefan–Boltzmann constant, and T_s is the skin temperature (K). Time-varying (e.g., 0.5-h interval) surface albedos α were derived by $\alpha = 1.4/(1.0 + 0.4\mu)\alpha_c$, where $\alpha_c = 0.16$ and μ is the cosine of the solar zenith angle (Briegleb 1992).

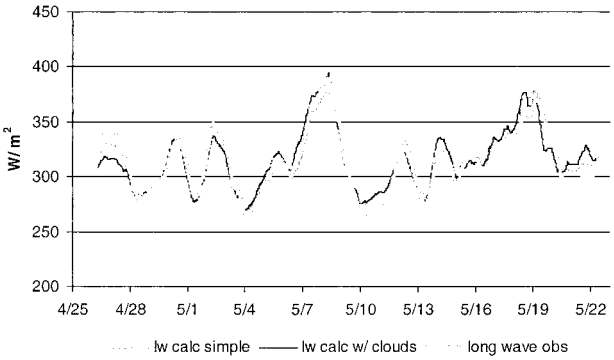

FIG. 11. Comparison of computed longwave downward radiation vs observed (long wave obs) at site 7, given as a 24-h moving average between 26 Apr and 22 May. The light, dashed line, labeled ''lw calc simple'' is according to the simple energy balance of Eq. (1), and the dark line labeled ''lw calc w/ clouds'' used Eqs. (1)–(4) to compute longwave downward radiation.

For station 9, both longwave downward and shortwave downward radiation were computed from a set of empirical relationships based on clear-sky solar radiation, air and skin temperatures, vapor pressure, and an estimate of cloud-cover fraction. The cloud-cover fraction f was computed so that the surface radiation budget [Eq. (1)] was balanced at each time step. Downward longwave radiation was determined empirically from Brutsaert (1982),

$$L_d = 1.24\left(\frac{e_a}{T_a}\right)^{1/7} \sigma T_a^4(1 + 0.22f^2), \tag{2}$$

where e_a is vapor pressure (hPa) and T_a is the daily air temperature near the ground (K), given as a 24-h moving average for the given point in time. An estimate of upward longwave radiation based on surface measurements and estimates of incoming longwave radiation was given as

$$L_u = \varepsilon_s \sigma T_s^4 - (1 - \varepsilon_s)L_d. \tag{3}$$

Downward shortwave radiation was computed from clear-sky solar radiation S_c and a linear fraction of cloud cover,

$$S_d = S_c[0.3 + 0.7(1 - f)]. \tag{4}$$

Figure 11 is a plot of the observed and modeled 24-h moving average of longwave downward radiation for site 7 using both the simple energy balance of Eq. (1) and the cloud-based energy balance of Eqs. (1)–(4). The moving average was plotted to filter the variance in the L_d signal to assess the quality of the modeled versus observed values. The plot shows good agreement between measured and estimated longwave downward radiation (the maximum difference being less than 30 W m^{-2}) for the period of 25 April–22 May. Where appropriate, one of these methods was applied to the data at each site to create a continuous time series of L_d.

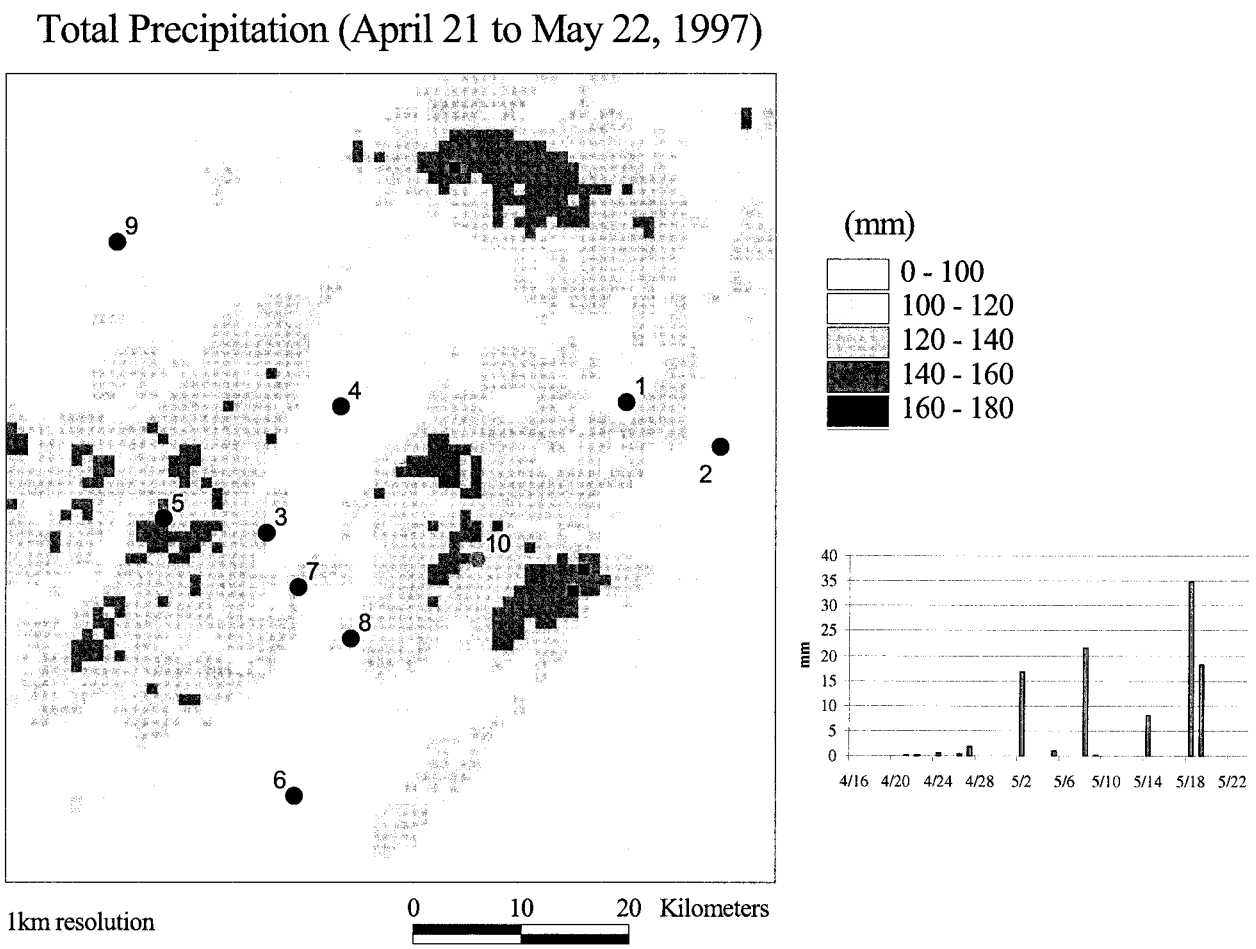

FIG. 12. Total precipitation accumulation from gauge-corrected radar during the CASES-97 experiment at 1-km spatial resolution. The inset time series is a plot of the daily precipitation total for the entire domain.

b. Precipitation

Gridded, half-hourly precipitation was derived from two radar-based sources and then adjusted to match data from the installed gauge network (Fig. 12). NCAR's dual-polarization S-Pol radar was operational during three major rainfall events of 2, 8, and 18 May 1997 (Brandes 1998). Gauge-corrected precipitation estimates from the S-Pol radar were available in a spherical coordinate system with a horizontal resolution of 150 m at 1° azimuth intervals and a temporal resolution of approximately 2 min. For the three events of 2, 8, and 18 May, these data were then resampled to the grid spacings of 1, 5, and 10 km using a bilinear interpolation. Half-hour accumulations of the 2-min data were simultaneously computed during the spatial aggregation process.

Where S-Pol data were not available, gauge-corrected (stage III) QPEs from Wichita's NEXRAD Weather Surveillance Radar-1988 Doppler (WSR-88D), at a spatial resolution of 4.7 km and at a 1-h temporal interval were used. The NEXRAD hourly estimates were simply halved to create half-hourly estimates and were rescaled to match the 1-, 5-, and 10-km grids. Comparisons between radar estimates and the gauge network precipitation values were made for the major rainfall events of 27 April, 2 May, 5 May, 8 May, and 18 May for both the NEXRAD and S-Pol QPEs. Although the radar QPEs are gauge corrected, the NEXRAD correction is done regionally and, therefore, exhibited local variations relative to gauge observations. Figure 13 are comparisons between the gauge totals and the radar estimates of precipitation and show good agreement. Note that NEXRAD rainfall estimates probably underestimated heavy rainfall events, but, fortunately, the three largest events were measured by S-Pol radar. Also of interest was the spatial variance of the precipitation over the CASES domain. The mean of the 32-day, accumulated half-hourly precipitation estimate for the 1-km grid (5254 points) was 109 mm, with a standard deviation of 22 mm, giving a coefficient of variation of 0.20.

c. Gridded atmospheric forcing dataset

From the surface flux station data, we developed a uniformly distributed, multiscale (with spatial resolu-

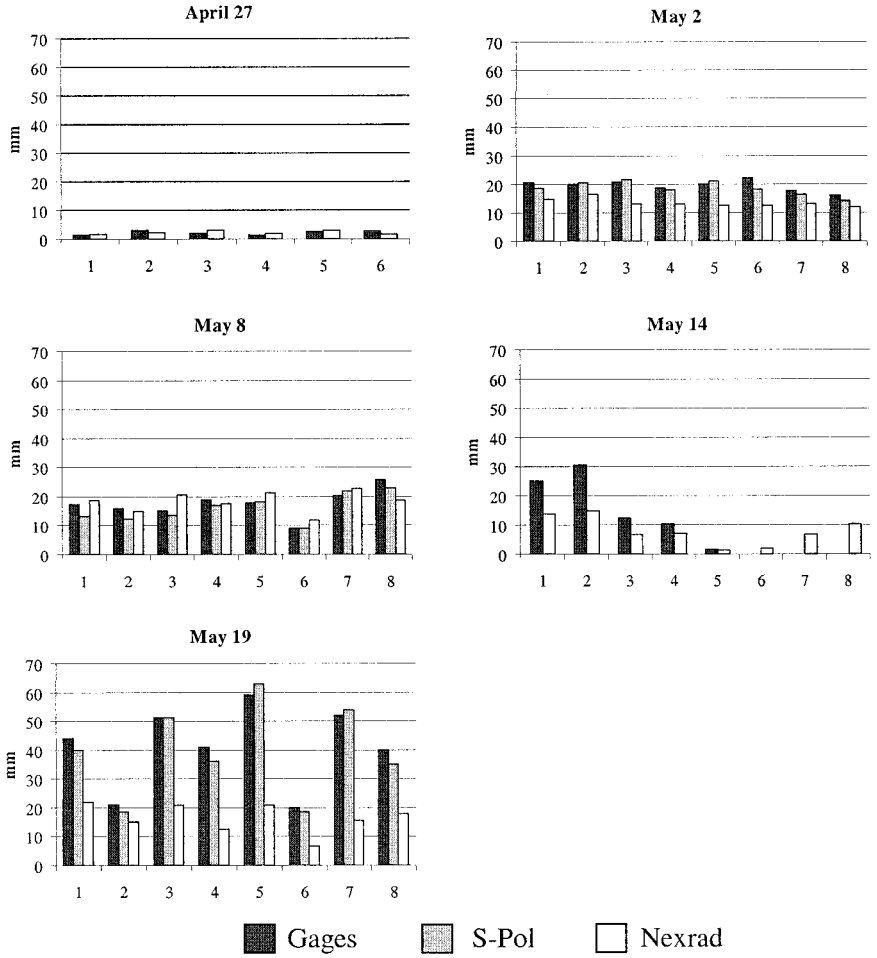

FIG. 13. Comparison of the NEXRAD WSR-88D and S-Pol radar-derived precipitation estimates with rain gauge estimates at surface flux stations 1–8.

tions of 1, 5, and 10 km), and time-varying (half hourly) comprehensive atmospheric forcing dataset covering a 74 km × 71 km area for the period from 0000 UTC 21 April to 2345 UTC 22 May 1997 (available online at http://www.rap.ucar.edu). A two-dimensional minimum curvature spline was used to interpolate the point data to a grid, which preserved the observation, ensuring data consistency. This scheme is similar to the multiquadric interpolation scheme that was shown by Nuss and Titley (1994) to be superior to common methods such as the Barnes or Cressman interpolation schemes. The geographic coordinates of the domain are a minimum latitude and longitude of 37.193°N, 97.311°W, respectively, in the lower left corner and a maximum latitude and (easternmost) longitude of 37.877° N, 96.494° W, respectively. For the transformation of the station data to a regular, equal area grid, the domain was projected to a Universal Transverse Mercator projection.

The NOAA surface flux station (site 10) was used to compare gridded estimates with independent observations of net radiation (only net radiation was measured at site 10) and 2-m air temperature. A comparison of observations at station 10 with the spatially interpolated estimates at that same point shows close agreement, with low bias (rmse for radiation: 27 W m^{-2}; rmse for 2-m air temperature: 0.8°C) and high correlation (variance R^2 for net radiation: 0.983; R^2 for 2-m air temperature: 0.989). The differences in interpolated versus observed values of net radiation were slightly greater than those of 2-m air temperature, because solar radiation exhibits greater within day variance due to the changing cloud cover. The site-10 interpolated values of net radiation showed a consistent bias, in which daytime interpolated values were consistently higher than and nighttime interpolated values were consistently lower than those observed at site 10.

Station 4 was used to perform an independent check of the spatial interpolation scheme. This site's data were first removed from the array of station data, and then the time-varying grids were reinterpolated, but now using only stations 1–3 and 5–9, inclusive. Interpolated estimates of site-4 data were then extracted and compared with site-4 observations. The estimated 2-m air temperature at site 4 closely matched the observed series

($R^2 = 0.978$; rmse = 0.6°C). A comparison of observed versus interpolated values of solar radiation showed greater differences, but with fairly uniform scatter and little bias ($R^2 = 0.967$; rmse = 24 W m^{-2}). Again, the spatial variability of solar radiation is greater, largely from cloud-cover variations.

d. Variance between station data

The degree of spatial variance in the atmospheric forcing maps at the 1-, 5-, and 10-km resolutions is only as great as the variance that exists in the original station data. Therefore, the station data were analyzed for their degree of variability by applying a rotated, principal component analysis (PCA) approach. PCA is a common technique in meteorology to characterize the most important spatial modes of variability [for a detailed discussion of the PCA technique, review Preisendorfer (1991)].

The PCA method was used to examine the extent of the subgrid-scale heterogeneity at the land surface of four representative atmospheric variables, 1) 2-m air temperature, 2) net radiation, 3) air pressure, and 4) specific humidity. To eliminate any bias in the PCA results due to the summer warm-up period, each series was linearly detrended. Then, the diurnal variability was removed by subtracting out the average half-hourly value from the 32-day time series for each select variable. In this way, the focus of the comparison was only on the standardized variability for each of the four series.

The contours in Fig. 14 are the PCA loadings of the first principal component for the given atmospheric variable. Each plot suggests the relative contribution of each site to the total observed variance over the entire domain. By contouring the site loadings, a sense of the degree of spatial variability in the final, time-varying, gridded dataset is achieved. The magnitudes of the individual contours are less important than their relative differences. If the loading values of the component are nearly equal (hence fewer contours), then each site contributed a near-equal amount to the total variance over the domain. This would also suggest little variance between the sites and high cross correlations. Greater site-to-site differences in the magnitude of the loadings suggest that each site contributed a different amount to the total variance over the domain. In this case, the contour gradients would be steeper and there would be greater site-to-site variability and lower cross correlations.

Not surprising, the air pressure and specific humidity did not show as significant variability from station to station as did net radiation and air temperature. The contour gradients of the loading for air pressure and specific humidity are small in comparison with those of the air temperature and net radiation. Although there is a surprising amount of variability shown in the air temperature loading map, a close examination of air temperature in Fig. 14 shows that the loading gradient is largely due to the contribution from sites 1 and 2. These two sites were more than 30 km from the others and in an area with more topographic variability and higher elevations. The maps in Fig. 14 also point to a data deficiency in the northeastern part of the study domain, because there is little to no gradient in the loading contours. It is regrettable that this area lacked a surface measuring station.

e. Gridded land surface and soil properties dataset

Surface datasets of 1, 5, and 10 km were created to coincide with the atmospheric forcing dataset and were composed of 1-km State Soil Geographic Database (STATSGO) soil data (including soil water capacity, porosity, texture, class, etc.); 1-km U.S. Geological Survey/Earth Resources Observation Systems (USGS/EROS) vegetation data; 30-m state of Kansas Survey Land Use Data (KSLUD); and the USGS Digital Elevation Model data. The KSLUD depict 10 general land cover classes for Kansas and were compiled from a digital classification of Landsat Thematic Mapper (TM) imagery as part of the ''Core Database'' for the state of Kansas. These data were developed from the Landsat image for 1993. Land cover class types are given as integer values, with a range between 1 and 10. Land cover class names and their associated integer identifier include residential (1), commercial/industrial (2), urban grassland (3), urban woodland (4), urban water (5), cropland (6), grassland (7), woodland, (8), water (9), and other (10).

6. Summary

The different approaches to represent subgrid-scale variability effects in atmospheric–hydrological models has recently been an area of focused research, yet verification and assessment of these methods has been inadequate because of a lack of validation data. The 1997 Cooperative Atmosphere–Surface Exchange Study experiment provided an excellent opportunity to address this problem by developing a multiscale dataset of atmospheric, surface, and subsurface observations that covered a region with a scale order comparable to mesoscale models and GCMs. The CASES-97 experiment consisted of surface flux measurement stations, as well as weather radar, sodar profilers, rawinsondes, and aircraft platforms. This paper focused on the surface flux measurement stations, by looking at the heat flux response of the stations in relation to their land cover types and atmospheric forcing, and the development of a gridded dataset to aid in validation studies of various land–atmosphere schemes.

A significant amount of variance in the 6-h, daytime average of sensible and latent heat was from radiation fluctuations due to cloud cover. However, the type of land cover and its specific characteristics, changes in soil moisture, and other factors also contributed to heat flux variance at and among the different sites. The var-

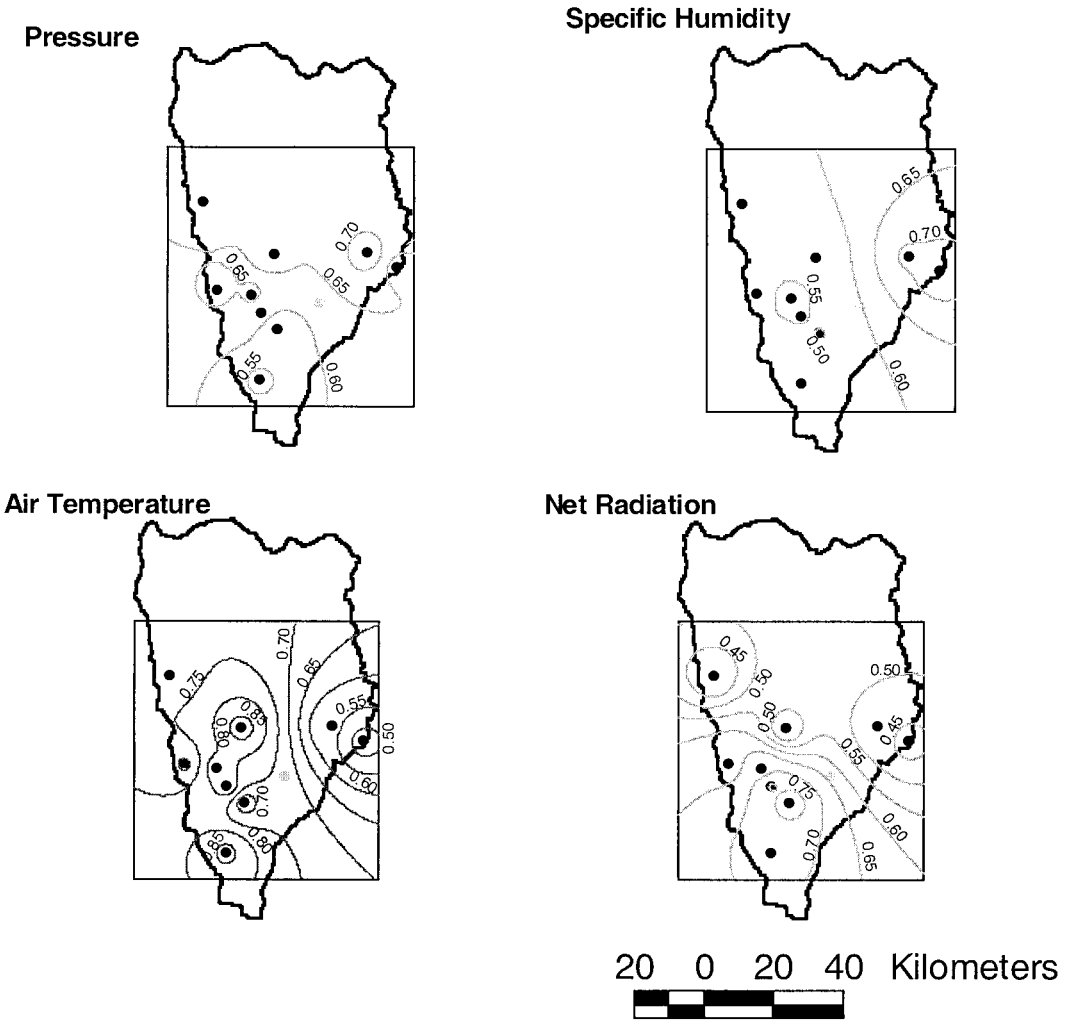

FIG. 14. The loadings of the first component of the orthogonally rotated PCA for the select atmospheric variable. Only the first component (or factor) is shown, because other components did not yield additional insights.

iability of the latent heat flux was more sensitive to the characteristics of the vegetation, whereas the sensible heat flux for the same vegetation was less sensitive to the specific vegetation charactersitics. It is regretable that measurement errors of various surface heat flux constituents led to a surface energy imbalance.

In agreement with Smith et al. (1992), the cloud-induced flux variance for a composited set of days was a major factor in statistically characterizing the areawide surface fluxes. When cloudy days were included in the computation of an average ''day,'' there was more variance when compared with an average day based only on cloud-free days.

Although there was significant spatial variability of the surface heat fluxes, the scaling results suggested that, when deriving a composite diurnal cycle of area-averaged fluxes, this variability was largely attenuated. The site-to-site variance in latent and sensible heat flux was effectively canceled during the area-averaging process, suggesting that fluxes scale linearly when creating a composite cycle over many days. There was significant site-to-site variability of surface fluxes, both for sites with the same land cover and for sites with differing land cover, but when these sites were combined to produce a composite, area-averaged diurnal cycle, the mean and variance did not significantly depend on their proportional weighting.

The greening process and related photosynthetic activity were shown to control the latent heat flux response, especially for the grass sites. During the early days of the experiment, the relatively ''inactive'' grass layer acted as a shield and prevented shortwave radiation from reaching the wet ground surface, with this inactive vegetation reducing the turbulent diffusion of water vapor from the ground surface to the atmosphere (Bougeault 1991).

Surface fluxes were partially controlled by the surface characteristics, topography, available soil moisture, pho-

tosynthetic activity, and so on. How these small-scale features influence area-averaged heat flux is of interest, but reproducing detailed spatial patterns using point values from site measurements is not possible, because the scale of variability of surface fluxes is small relative to the scale defined by the separation of sites. Therefore a spatially distributed, time-varying dataset of atmospheric forcing data was developed for use in numerical land surface models to address further the issue of horizontal variability of surface fluxes.

Static grids of land surface characteristics (e.g., land cover and soil properties) and half-hourly grids of atmospheric forcing data at spatial resolutions of 1, 5, and 10 km over an appproximate 74 km $\times$ 71 km area of the Walnut watershed were created. With the exception of precipitation, these uniform grids were generated from the CASES-97 flux-measuring stations by applying a minimum-curvature spline interpolation scheme to these station data. This technique was shown to reproduce estimates of the atmospheric forcing variables such as 2-m air temperature, solar radiation, and pressure adequately. The precipitation field was developed from two gauge-corrected weather radars, the NEXRAD WSR-88D and NCAR's S-Pol radar. Although the atmospheric forcing conditions, based on the nine surface stations, may lack signficant heterogenity in the 1-km gridded dataset over the 74 km $\times$ 71 km area, the introduction of high-resolution precipitation data can preserve the desired surface variability in rainfall and moisture. A gridded surface dataset, which spatially corresponds to the gridded atmospheric forcing dataset, was created to support land surface modeling exercises. These data included soil types and texture, soil hydraulic properties at varying depths, and land use and land cover descriptions.

Future work will involve the use of several widely used land surface models in generating multiscale surface heat flux maps for better assessing the role of surface heterogenity on area-averaged heat fluxes.

Acknowledgments. This research was supported through NASA Research Grant NAG5-7541 under the Water Applications Program in the Office of Earth Sciences. See Lemone et al. (2000) for additional acknowledgments and contributions to CASES-97. The constructive comments of three anonymous reviewers were tremendously helpful.

REFERENCES

Avissar, R., and R. A. Pielke, 1989: A parameterization of heterogeneous land surfaces for atmospheric numerical models and its impact on regional meteorology. *Mon. Wea. Rev.,* **117,** 2113–2136.

——, and F. Chen, 1993: Development and analysis of prognostic equations for mesoscale kinetic energy and mesoscale (subgrid-scale) fluxes for large-scale atmospheric models. *J. Atmos. Sci.*, **50,** 3751–3774.

——, and T. Schmidt, 1998, An evaluation of the scale at which ground-surface heat flux patchiness affects the convective boundary layer using large-eddy simulations. *J. Atmos. Sci.,* **55,** 2666–2689.

Betts, A. K., S. Y. Hong, and H. L. Pan, 1996: Comparison of NCEP/NCAR reanalysis with 1987 FIFE data. *Mon. Wea. Rev.,* **124,** 1480–1498.

Bonan, G. B., D. Pollard, and S. L. Thompson, 1993: Influence of subgrid-scale heterogenity in leaf area index, stomatal resistance, and soil moisture on grid-scale land–atmospheric interactions. *J. Climate,* **6,** 1882–1897.

Bougeault, P., 1991: Parameterization schemes of land surface processes for mesocale atmospheric models, *Land Surface Evaporation: Measurement and Parameterization,* T. Schmugge and J. Andre, Eds., Springer-Verlag, 80 pp.

Brandes, E. A., J. Vivekanandan, and J. W. Wilson, 1998: A comparison of radar reflectivity estimates of rainfall from collocated radars. *J. Atmos. Oceanic Technol.,* **16,** 1264–1272.

Briegleb, B. P., 1992: The delta-Eddington approximation for solar radiation in the NCAR Community Climate Model. *J. Geophys. Res.,* **97,** 7603–7612.

Brutsaert, W., 1982: *Evaporation into the Atmosphere: Theory, History, and Applications.* D. Reidel Publishing, 299 pp.

Carlson, T., R. Gilles, and T. Schmugge, 1995: An interpretation of methodologies for indirect measurement of soil water content. *Agric. For. Meteor.,* **77,** 191–205.

Charney, J., W. J. Quirk, S.-H. Chow, and J. Kornfield, 1977: A comparative study of the effects of albedo change on drought in semiarid regions. *J. Atmos. Sci.,* **34,** 1366–1385.

Chen, F., and R. Avissar, 1994a: The impact of land surface wetness heterogeneity on mesocale heat fluxes. *J. Appl. Meteor.,* **33,** 1323–1340.

——, and ——, 1994b: The impact of shallow convective moist processes on mesoscale heat fluxes. *J. Appl. Meteor.,* **33,** 1382–1401.

——, Z. Janjic, and K. Mitchell, 1997: Impact of atmospheric surface layer parameterization in the new land-surface schemes of the NCEP Mesoscale Eta Numerical Model. *Bound.-Layer Meteor.*, **85,** 391–421.

——, K. Mitchell, Z. Janjic, and M. Baldwin, 1998: Impact of land surface processes on the NCEP Eta Model quantitative precipitation forecast. Preprints, *Special Symp. on Hydrology.* Phoenix, AZ, Amer. Meteor. Soc., 281–282.

Claussen, M., 1991: Estimation of areally-averaged surface fluxes. *Bound.-Layer Meteor.,* **54,** 387–410.

Doran, J. C., J. M. Hubbe, J. C. Liljegren, W. J. Shaw, G. J. Collatz, D. R. Cook, and R. L. Hart, 1998: A technique for determining the spatial and temporal distributions of surface fluxes of heat and moisture over the Southern Great Plains Cloud and Radiation Testbed. *J. Geophys. Res.,* **103,** 6109–6121.

Entekhabi, D., and P. S. Eagleson, 1989: Land surface hydrology parameterization for atmospheric general circulation models including subgrid scale variability. *J. Climate,* **2,** 817–831.

Famiglietti, J. S., and E. F. Wood, 1991: Evapotranspiration and runoff from large land areas: Land surface hydrology for atmospheric general circulation models. *Surv. Geophys.,* **12,** 179–204.

Gao, W., 1995: Parameterization of subgrid-scale land surface fluxes with emphasis on distributing mean atmospheric forcing using satellite-derived vegetation index. *J. Geophys. Res.,* **100,** 14 305–14 317.

Garratt, J. R., R. A. Pielke, W. F. Miller, and T. J. Lee, 1990: Mesocale model response to random, surface-based perturbations—a seabreeze experiment. *Bound.-Layer Meteor.,* **52,** 313–334.

Ghan, S. J., J. C. Liljegren, W. J. Shaw, J. H. Hubbe, and J. C. Doran, 1997: Influence of subgrid variability on surface hydrology. *J. Climate*, **10,** 3157–3167.

Goutorbe, J. 1991: A critical assessment of the Samer network accuracy. *Land Surface Evaporation: Measurement and Parameterization,* T. Schmugge and J. André, Eds., Springer-Verlag, 171–182.

Grotzner, A., R. Sausen, and M. Claussen, 1996: The impact of sub-

grid scale sea-ice inhomogenities on the performance of the atmospheric general circulation model ECHAM3. *Climate Dyn.,* **12,** 477–496.

Horst, T. W., and S. P. Oncley: 1995: Flux-PAM measurement of scalar fluxes using cospectral similarity. Preprints, *Ninth Symp. on Meteorological Observations and Instrumentation,* Charlotte, NC, Amer. Meteor. Soc., 495–500.

Koster, R. D., and M. J. Suarez, 1992: Modeling the land surface boundary in climate models as a composite of independent vegetation stands. *J. Geophys. Res.,* **97,** 2697–2715.

Lakhtakia, M. N., and T. T. Warner, 1994: A comparison of simple and complex treatments of surface hydrology and thermodynamics suitable for mesoscale atmospheric models. *Mon. Wea. Rev.,* **122,** 880–896.

LeMone, M. A., and Coauthors, 1998: CASES-97: Diurnal variation of the fair-weather PBL. Preprints, *Special Symp. on Hydrology.* Phoenix, AZ, Amer. Meteor. Soc., 88–92.

——, and Coauthors, 2000: Land–atmosphere interaction research: Early results and opportunities in the Walnut River watershed in southeast Kansas: CASES and ABLE. *Bull. Amer. Meteor. Soc.,* **81,** 757–779.

Li, B., and R. Avissar, 1994: The impact of spatial variability of land-surface characteristics on land-surface heat fluxes. *J. Climate,* **7,** 527–537.

Liang, X., D. P. Lettenmaier, E. F. Wood, and S. J. Burges, 1994: A simple hydrologically based model of land surface water and energy fluxes for general circulation models. *J. Geophys. Res.,* **99,** 14 415–14 428.

Nuss, W. A., and D. W. Titley: 1994: Use of multiquadric interpolation for meteorological objective analysis. *Mon. Wea. Rev.,* **122,** 1611–1631.

Pan, H., and L. Mahrt, 1987: Interaction between soil hydrology and boundary-layer development. *Bound.-Layer Meteor.,* **38,** 185–202.

Pielke, R. A., G. A. Dalu, J. S. Snook, T. J. Lee, and T. G. F. Kittel, 1991: Nonlinear influence of mesoscale land use on weather and climate. *J. Climate,* **4,** 1053–1069.

Preisendorfer, R., 1991: *Principal Component Analysis in Meteorology and Oceanography.* Elsevier.

Schaake, J. C., V. I. Koren, Q.-Y. Duan, K. Mitchell, and F. Chen, 1996: A simple water balance model for estimating runoff at different spatial and temporal scales. *J. Geophys. Res.,* **101,** 7461–7457.

Segal, M., R. Avissar, M. C. McCumber, and R. A. Pielke, 1988: Evaluation of vegetation effects on the generation and modification of mesocale ciruclations. *J. Atmos. Sci.,* **45,** 2268–2292.

Sellers, P. J., and Coauthors, 1995: Effects of spatial variability in topography, vegetation cover and soil moisture on area-averaged surface fluxes: A case study using the FIFE 1989 data. *J. Geophys. Res.,* **100,** 25 607–25 629.

Shen, S., and M. Y. Leclerc, 1995: How large must surface inhomogenities be before they influence the convective boundary layer? A case study. *Quart. J. Roy. Meteor. Soc.,* **121,** 1209–1228.

Smith, E. A., and Coauthors, 1992: Area-averaged surface fluxes and their time-space variability over the FIFE experimental domain. *J. Geophys. Res.,* **97,** 18 599–18 622.

Wang, M., and J. Paegle, 1996: Impact of analysis uncertainty upon regional atmospheric moisture flux. *J. Geophys. Res.,* **101,** 7291–7303.

Wood, E. F., and E. Lakshmi, 1993: Scaling water and energy fluxes in climate systems: Three land–atmospheric modeling experiments. *J. Climate,* **6,** 839–857.

——, D. P. Lettenmaier, and V. G. Zartarian, 1992: A land surface parameterization with subgrid variability for general circulation models. *J. Geophys. Res.,* **97,** 2717–2728.

Yan, H., and R. A. Anthes, 1988: The effect of variations in surface moisture on mesoscale circulations. *Mon. Wea. Rev.,* **116,** 192–208.

Zhong, S., and J. C. Doran, 1998: An evaluation of the importance of surface flux variability on GCM-scale boundary layer characteristics using realistic meteorological and surface forcing. *J. Climate,* **11,** 2774–2788.